

An Interpretable Representation Learning Approach for Diffusion Tensor Imaging

Vishwa Mohan Singh^{*1,2} 

Alberto Gaston Villagran Asiales²

Luisa Sophie Schuhmacher²

Kate Rendall^{*2}

Simon Weißbrod^{*2}

David Rügamer^{1,3}

Inga Körte^{2,4}

VISHWA.SINGH@MED.UNI-MUENCHEN.DE

ALBERTO.VILLAGRAN@MED.UNI-MUENCHEN.DE

LUISA.SCHUHMACHER@MED.UNI-MUENCHEN.DE

KATE.RENDALL@MED.UNI-MUENCHEN.DE

SIMON.WEISSBROD@MED.UNI-MUENCHEN.DE

DAVID.RUEGAMER@STAT.UNI-MUENCHEN.DE

INGA.KOERTE@MED.UNI-MUENCHEN.DE

¹ Institut für Statistik, Ludwig-Maximilians-Universität, Munich, Germany

² cBRAIN, Department of Child and Adolescent Psychiatry, Psychosomatics, and Psychotherapy, Ludwig-Maximilians-Universität, Munich, Germany.

³ Munich Center for Machine Learning, Munich, Germany.

⁴ Department of Psychiatry, Psychiatry Neuroimaging Laboratory, Brigham and Women's Hospital, Harvard Medical School, Boston, MA, USA.

Editors: Accepted for publication at MIDL 2025

Abstract

Diffusion Tensor Imaging (DTI) tractography offers detailed insights into the structural connectivity of the brain, but presents challenges in effective representation and interpretation in deep learning models. In this work, we propose a novel 2D representation of DTI tractography that encodes tract-level fractional anisotropy (FA) values into a 9×9 grayscale image. This representation is processed through a Beta-Total Correlation Variational Autoencoder (β -TCVAE) with a Spatial Broadcast Decoder to learn a disentangled and interpretable latent embedding. We evaluate the quality of this embedding using supervised and unsupervised representation learning strategies, including auxiliary classification, triplet loss, and SimCLR-based contrastive learning. Compared to the 1D Group deep neural network (DNN) baselines, our approach improves the F1 score in a downstream sex classification task by 15.74% and shows a better disentanglement than the 3D representation.

Keywords: Diffusion Tensor Imaging, Autoencoders, Representation Learning

1. Introduction

Diffusion Tensor Imaging (DTI) tractography is a non-invasive technique that models white matter fiber bundles in the brain (Buyanova and Arsalidou, 2021; Jelescu and Budde, 2017). It has become increasingly crucial for studying neurodevelopment, aging, and neurological diseases (Sundgren et al., 2004). However, effectively representing the complex geometry and connectivity information in DTI tractography remains a challenge in analysis. Methodologies using 1-dimensional representation often disregard spatial context, while the complex 3D architecture lacks interpretability (Related works in Appendix B).

To address this, we propose a novel 2D representation of DTI tractography that maintains critical spatial information while remaining amenable to deep learning techniques.

* Contributed equally

Specifically, we transform tract-level fractional anisotropy (FA) values into a 9×9 grid format, where each pixel encodes the FA value of one tract. From this grid, we learn a disentangled class-aware latent representation using a combination of a Disentangled Variational Autoencoder and representation learning strategies. This representation is meant to be used in a late-fusion multi-modal architecture to analyze different MRI Modalities.

2. Methodology

2.1. Dataset and Representation

Data was collected from young adult amateur soccer players with at least 5 years of organized training (46 males and 23 females), and control athletes engaged in non-contact sports (11 males and 25 females). On this, we use sex classification as our downstream task. For postprocessing, we use WMA800 (O'Donnell and Westin, 2007; O'Donnell et al., 2012) to divide the white matter fibers into 74 different anatomical tracts based on the ORG-800FC-100HCP atlas (Zhang et al., 2018).

We convert this WMA output to a compact 2D representation of DTI tractography. The 74 tracts are arranged in a 9×9 grid using Multi-Dimensional Scaling (Mead, 1992) to preserve distance. After finding the grid coordinates, we use the Hungarian algorithm to solve the overlap between several centroids (See Appendix Algorithms 1 and 2).

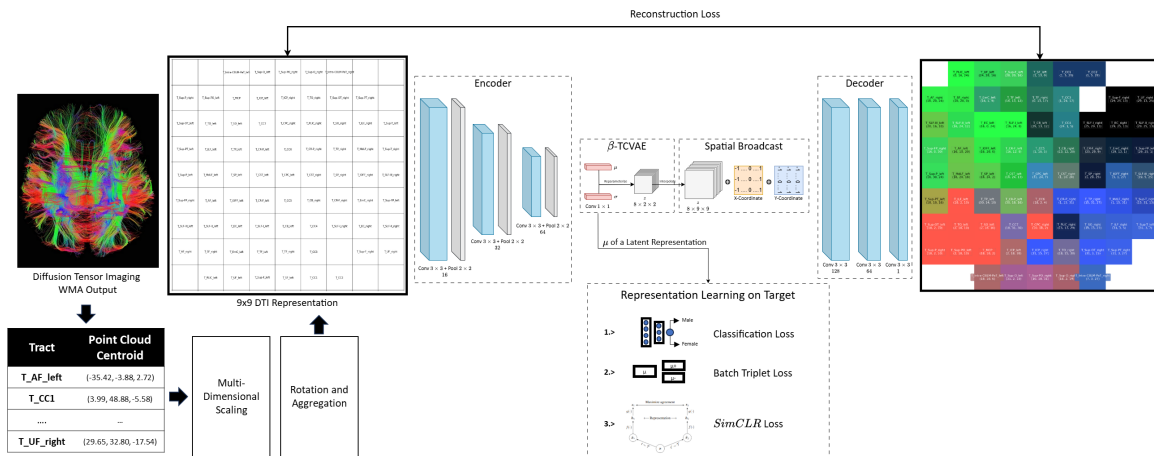


Figure 1: Architecture to convert the Dense DTI representation to an interpretable latent vector Z . The representation learning and classification are performed on the estimated mean μ . The reconstruction shows latent values, which are the explainers for each tract.

2.2. Autoencoder and Representation Learning

The core of our model is a variational autoencoder (Kingma et al., 2013). The encoder compresses the 9×9 FA image into a latent vector of size 32 and a spatial broadcast de-

coder (Watters et al., 2019) to make the latent vector retain spatial coherence. The model is trained using a β -TCVAE loss, which encourages disentanglement by penalizing total correlation (Chen et al., 2018).

To retain class-relevant information in the latent space, we evaluate three strategies: a supervised auxiliary classifier as a proxy for semantic structure, a triplet loss for preserving local class-wise distances (Hoffer and Ailon, 2015), and an unsupervised SimCLR loss for learning global latent structure (Chen et al., 2020). The full architecture is shown in Figure 1.

3. Experiment and Results

The following Table 1 shows the results from the models tested. The Disentangled (Dis.) VAE in the table refers to the model that uses both spatial broadcasting and β -TCVAE loss. As controls, we use a 1D deep neural network (DNN), a 1D Grouped DNN, and a 3D Autoencoder, which works on the original centroid position. We compare the separability (Sep) of the latent space using a KNN classifier (Dyballa et al., 2024) with $k = 3$ and the metrics from the best classifier from LazyClassifier (Pandala and Silva, 2019). We measure the Mutual Information Gap (MIG) (Chen et al., 2018) of different regions to evaluate disentanglement.

Table 1: Comparisons of Models over classification performance, reconstruction, and Mutual Information Gap

Network	Accuracy	F1	Sep	Recon	MIG
1D-DNN	53.90 (± 12.2)	51.15 (± 28.4)	-	-	-
1D Group DNN	65.00 (± 14.0)	68.78 (± 15.7)	-	-	-
3D VAE + Aux	82.60 (± 9.4)	82.06 (± 9.7)	77.08	0.0190	0.0344
2D VAE + Aux	80.90 (± 9.5)	80.15 (± 10.1)	81.25	0.0159	0.0503
2D β -TCVAE + Aux	81.45 (± 13.5)	81.37 (± 13.4)	83.33	0.0151	0.0535
2D Dis. VAE + Aux	80.09 (± 8.6)	79.74 (± 9.5)	81.25	0.0180	0.0640
2D Dis. VAE + Triplet	77.27 (± 8.6)	77.30 (± 8.1)	81.25	0.0171	0.0739
2D Dis. VAE + SimCLR	81.72 (± 12.0)	81.42 (± 12.3)	70.81	0.0768	0.0588

4. Discussion and Conclusion

Along with better disentanglement than 3D, the 2D representation improves over the best 1D model by 12.64% in F1 score, with no significant drop from the 3D equivalent. Interpretation results from SHAP (Lundberg and Lee, 2017) show that across the subjects, the male subjects show a higher FA value, especially in the left Corona Radiata, Right Superior Longitudinal Fasciculus, and Right Corticospinal Tracts (refer Appendix E Figure 2). Some patterns shown in the interpretation align with the findings from previous DL and statistical analyses (Menzler et al., 2011; Chen et al., 2023).

Further improvements can be made to the architecture’s interpretability by finding a better balance of classification and the Kullback-Leibler term. Additionally, methods like

attention (Vaswani et al., 2017) or factorization machines (Rendle, 2010) could be used to model any interactions between the tracts.

References

Irina S Buyanova and Marie Arsalidou. Cerebral white matter myelination and relations to age, gender, and cognition: a selective review. *Frontiers in human neuroscience*, 15: 662031, 2021.

Ricky TQ Chen, Xuechen Li, Roger B Grosse, and David K Duvenaud. Isolating sources of disentanglement in variational autoencoders. *Advances in neural information processing systems*, 31, 2018.

Ting Chen, Simon Kornblith, Mohammad Norouzi, and Geoffrey Hinton. A simple framework for contrastive learning of visual representations. In *International conference on machine learning*, pages 1597–1607. PmLR, 2020.

Yuqian Chen, Fan Zhang, Leo R Zekelman, Tengfei Xue, Chaoyi Zhang, Yang Song, Nikos Makris, Yogesh Rathi, Weidong Cai, and Lauren J O’Donnell. Tractgraphcnn: anatomically informed graph cnn for classification using diffusion mri tractography. In *2023 IEEE 20th International Symposium on Biomedical Imaging (ISBI)*, pages 1–5. IEEE, 2023.

Luciano Dyballa, Evan Gerritz, and Steven W Zucker. A separability-based approach to quantifying generalization: which layer is best? *arXiv preprint arXiv:2405.01524*, 2024.

Yixue Feng, Bramsh Q Chandio, Sophia I Thomopoulos, Tamoghna Chattopadhyay, and Paul M Thompson. Variational autoencoders for generating synthetic tractography-based bundle templates in a low-data setting. In *2023 45th Annual International Conference of the IEEE Engineering in Medicine & Biology Society (EMBC)*, pages 1–6. IEEE, 2023.

Elad Hoffer and Nir Ailon. Deep metric learning using triplet network. In *Similarity-based pattern recognition: third international workshop, SIMBAD 2015, Copenhagen, Denmark, October 12-14, 2015. Proceedings 3*, pages 84–92. Springer, 2015.

Andrei Irimia, Xiaoyu Lei, Carinna M Torgerson, Zachary J Jacokes, Sumiko Abe, and John D Van Horn. Support vector machines, multidimensional scaling and magnetic resonance imaging reveal structural brain abnormalities associated with the interaction between autism spectrum disorder and sex. *Frontiers in computational neuroscience*, 12: 93, 2018.

Ileana O Jelescu and Matthew D Budde. Design and validation of diffusion mri models of white matter. *Frontiers in physics*, 5:61, 2017.

Diederik P Kingma, Max Welling, et al. Auto-encoding variational bayes, 2013.

Prince D Ngattai Lam, Gaetan Belhomme, Jessica Ferrall, Billie Patterson, Martin Styner, and Juan C Prieto. Trafic: fiber tract classification using deep learning. In *Medical Imaging 2018: Image Processing*, volume 10574, pages 257–265. SPIE, 2018.

Scott M Lundberg and Su-In Lee. A unified approach to interpreting model predictions. *Advances in neural information processing systems*, 30, 2017.

Al Mead. Review of the development of multidimensional scaling methods. *Journal of the Royal Statistical Society: Series D (The Statistician)*, 41(1):27–39, 1992.

K Menzler, M Belke, E Wehrmann, K Krakow, U Lengler, Andreas Jansen, Hajo M Hamer, Wolfgang H Oertel, Felix Rosenow, and Susanne Knake. Men and women are different: diffusion tensor imaging reveals sexual dimorphism in the microstructure of the thalamus, corpus callosum and cingulum. *Neuroimage*, 54(4):2557–2562, 2011.

Lauren J O’Donnell and Carl-Fredrik Westin. Automatic tractography segmentation using a high-dimensional white matter atlas. *IEEE transactions on medical imaging*, 26(11):1562–1575, 2007.

Lauren J O’Donnell, William M Wells III, Alexandra J Golby, and Carl-Fredrik Westin. Unbiased groupwise registration of white matter tractography. In *International Conference on Medical Image Computing and Computer-Assisted Intervention*, pages 123–130. Springer, 2012.

S.R. Pandala and Bruno Silva. Lazy predict project. <https://pypi.org/project/lazypredict/>, May 2019. Python package for quick evaluation of multiple machine learning models.

Gang Qu, Ziyu Zhou, Vince D Calhoun, Aiying Zhang, and Yu-Ping Wang. Integrated brain connectivity analysis with fmri, dti, and smri powered by interpretable graph neural networks. *ArXiv*, pages arXiv–2408, 2024.

Steffen Rendle. Factorization machines. In *2010 IEEE International conference on data mining*, pages 995–1000. IEEE, 2010.

Pia C Sundgren, Q Dong, D Gomez-Hassan, SK Mukherji, P Maly, and R Welsh. Diffusion tensor imaging of the brain: review of clinical applications. *Neuroradiology*, 46:339–350, 2004.

Scott Trinkle, Sean Foxley, Gregg Wildenberg, Narayanan Kasthuri, and Patrick La Rivière. The role of spatial embedding in mouse brain networks constructed from diffusion tractography and tracer injections. *Neuroimage*, 244:118576, 2021.

Ashish Vaswani, Noam Shazeer, Niki Parmar, Jakob Uszkoreit, Llion Jones, Aidan N Gomez, Łukasz Kaiser, and Illia Polosukhin. Attention is all you need. *Advances in neural information processing systems*, 30, 2017.

Nicholas Watters, Loic Matthey, Christopher P Burgess, and Alexander Lerchner. Spatial broadcast decoder: A simple architecture for learning disentangled representations in vaes. *arXiv preprint arXiv:1901.07017*, 2019.

Fan Zhang, Ye Wu, Isaiah Norton, Laura Rigolo, Yogesh Rathi, Nikos Makris, and Lauren J O’Donnell. An anatomically curated fiber clustering white matter atlas for consistent white matter tract parcellation across the lifespan. *Neuroimage*, 179:429–447, 2018.

Fan Zhang, Suheyla Cetin Karayumak, Nico Hoffmann, Yogesh Rathi, Alexandra J Golby, and Lauren J O’Donnell. Deep white matter analysis (deepwma): Fast and consistent tractography segmentation. *Medical image analysis*, 65:101761, 2020.

Yanfu Zhang, Liang Zhan, Shandong Wu, Paul Thompson, and Heng Huang. Disentangled and proportional representation learning for multi-view brain connectomes. In *Medical Image Computing and Computer Assisted Intervention–MICCAI 2021: 24th International Conference, Strasbourg, France, September 27–October 1, 2021, Proceedings, Part VII 24*, pages 508–518. Springer, 2021.

Appendix A. Availability of Code

The code used to generate these results is in the following anonymized public repository: https://anonymous.4open.science/r/DTI_2D_representation-0B47

Appendix B. Related Literature

The most common way to pair tractography output with machine learning has been 1D feature-based approaches using models like support vector machines (Irimia et al., 2018). These methods are computationally efficient and interpretable, but suffer from the loss of spatial and geometric information. TractGraphCNN (Chen et al., 2023) tries to address this by rearranging the fiber bundles in a graph. More expressive 3D alternatives like TRAFIC (Lam et al., 2018) and Deep White Matter Analysis (Zhang et al., 2020) representations, on the other hand, make the model harder to interpret.

Autoencoders, especially Variational Autoencoders (VAEs) (Kingma et al., 2013), have recently been used to learn low-dimensional embeddings from tractography data (Feng et al., 2023; Trinkle et al., 2021). Furthermore, studies integrating DTI with other modalities (e.g., fMRI, EEG) have demonstrated the importance of compact and interpretable embeddings for multimodal fusion (Qu et al., 2024; Zhang et al., 2021).

Appendix C. Mathematical Definitions of the Loss Function

The training objectives in our framework are built on the β -Total Correlation Variational Autoencoder (β -TCVAE) backbone, with three distinct variants depending on the auxiliary objective. The base β -TCVAE loss consists of a reconstruction term and a decomposed KL divergence that includes mutual information (MI), total correlation (TC), and dimension-wise KL. The total loss is given by:

$$\mathcal{L}_{\text{TCVAE}} = \mathcal{L}_{\text{recon}} + \mathcal{L}_{\text{KL}}, \quad (1)$$

where the reconstruction loss is defined as the mean squared error between the input x and the reconstruction \hat{x} :

$$\mathcal{L}_{\text{recon}} = \|x - \hat{x}\|_2^2. \quad (2)$$

The KL divergence is decomposed as:

$$\mathcal{L}_{\text{KL}} = \underbrace{\text{MI}(z; x)}_{\text{mutual information}} + \beta \cdot \underbrace{\text{TC}(z)}_{\text{total correlation}} + \underbrace{\sum_j D_{\text{KL}}(q(z_j) \| p(z_j))}_{\text{dimension-wise KL}}, \quad (3)$$

where β controls the strength of the disentanglement by scaling the total correlation term.

1. Auxiliary Classifier Loss: To guide the latent space with supervised signals, we add a binary cross-entropy loss from an auxiliary classifier f_{cls} operating on the latent mean μ . The total loss becomes:

$$\mathcal{L}_{\text{AE+Cls}} = \lambda_{\text{VAE}} \cdot \mathcal{L}_{\text{TCVAE}} + \lambda_{\text{Cls}} \cdot \mathcal{L}_{\text{BCE}}(f_{\text{cls}}(\mu), y), \quad (4)$$

where y is the ground truth label and λ_{Cls} balances the classification loss.

2. Triplet Loss: To structure the latent space based on local class similarity, we apply a batch-hard triplet loss on the latent mean μ , enforcing separation between positive and negative pairs:

$$\mathcal{L}_{\text{AE+Triplet}} = \lambda_{\text{VAE}} \cdot \mathcal{L}_{\text{TCVAE}} + \lambda_{\text{Triplet}} \cdot \mathcal{L}_{\text{Triplet}}(\mu, y), \quad (5)$$

where $\mathcal{L}_{\text{Triplet}}$ is defined as:

$$\mathcal{L}_{\text{Triplet}} = \max(0, \|\mu_a - \mu_p\|_2^2 - \|\mu_a - \mu_n\|_2^2 + \alpha), \quad (6)$$

with anchor μ_a , positive μ_p , negative μ_n , and margin α .

3. SimCLR Contrastive Loss: For unsupervised structure in the latent space, we apply the SimCLR loss on pairs of augmentations x_1, x_2 passed through the encoder, using the latent mean μ as the representation. The combined loss is:

$$\mathcal{L}_{\text{AE+SimCLR}} = \lambda_{\text{VAE}} \cdot \mathcal{L}_{\text{TCVAE}} + \lambda_{\text{SimCLR}} \cdot \mathcal{L}_{\text{SimCLR}}(\mu_1, \mu_2), \quad (7)$$

where the SimCLR loss is defined as:

$$\mathcal{L}_{\text{SimCLR}} = -\log \frac{\exp(\text{sim}(\mu_1, \mu_2)/\tau)}{\sum_{j=1}^{2N} 1_{[j \neq i]} \exp(\text{sim}(\mu_i, \mu_j)/\tau)}, \quad (8)$$

with cosine similarity $\text{sim}(\cdot, \cdot)$ and temperature parameter τ .

Each of these loss formulations guides the latent representation toward a specific structure—semantic separability, local neighborhood coherence, or augmentation invariance—while maintaining reconstruction quality and disentanglement through the β -TCVAE framework.

Appendix D. Algorithm for Rearrangement

To create a compact and spatially meaningful 2D representation of DTI tractography, we project 3D tract centroids onto a 2D grid. Algorithm 1 outlines the procedure, which first applies Multi-Dimensional Scaling (MDS) to preserve inter-tract distances, followed by normalization to fit the projected coordinates within a 9×9 grid. This forms the basis for consistent tract placement across subjects.

Algorithm 1: Convert DTI 3D Representation to 2D Grid

Input: $X = \{x_1, x_2, \dots, x_n\}$, where $x_i \in \mathbb{R}^3$ (3D data points)**Output:** $G = \{g_1, g_2, \dots, g_n\}$, where $g_i \in \{1, \dots, 9\} \times \{1, \dots, 9\}$ (2D grid positions)**Step 1: Dimensionality Reduction via MDS;** $Y \leftarrow \text{MDS}(X, d = 2);$ **Step 2: Normalize 2D Coordinates to a 9x9 Grid;**Compute $y_{\min,1}$ and $y_{\max,1}$, the minimum and maximum of the first coordinates in Y ;Compute $y_{\min,2}$ and $y_{\max,2}$, the minimum and maximum of the second coordinates in Y ;**for** each point $y_i = (y_{i,1}, y_{i,2}) \in Y$ **do** $g_{i,1} \leftarrow \text{round}\left(\frac{y_{i,1} - y_{\min,1}}{y_{\max,1} - y_{\min,1}} \times 8\right) + 1;$ $g_{i,2} \leftarrow \text{round}\left(\frac{y_{i,2} - y_{\min,2}}{y_{\max,2} - y_{\min,2}} \times 8\right) + 1;$ $g_i \leftarrow (g_{i,1}, g_{i,2});$ **end****Step 3: Rearrangement using the Hungarian Algorithm;**Construct a cost matrix $C \in \mathbb{R}^{n \times n}$ where $C(i, j)$ is the distance between g_i and the j th grid position; $P \leftarrow \text{HungarianAlgorithm}(C);$ Reassign each point y_i to the grid position indicated by P ;**return** G ;

To resolve overlapping grid positions resulting from the MDS projection, we use the Hungarian Algorithm to optimally assign tracts to unique 2D locations while minimizing displacement. Algorithm 2 summarizes this process, ensuring a one-to-one mapping of tracts to grid positions with minimal distortion of spatial relationships.

Algorithm 2: HungarianAlgorithm

Input: $C \in \mathbb{R}^{n \times n}$, the cost matrix**Output:** P , the optimal assignment mapping each row to a column**Step 1: Row Reduction;****for** $i \leftarrow 1$ **to** n **do** $minRow \leftarrow \min\{C(i, j) : 1 \leq j \leq n\};$ **for** $j \leftarrow 1$ **to** n **do** $| C(i, j) \leftarrow C(i, j) - minRow;$ **end****end****Step 2: Column Reduction;****for** $j \leftarrow 1$ **to** n **do** $minCol \leftarrow \min\{C(i, j) : 1 \leq i \leq n\};$ **for** $i \leftarrow 1$ **to** n **do** $| C(i, j) \leftarrow C(i, j) - minCol;$ **end****end****Step 3: Cover Zeros with Minimum Number of Lines;**Cover all zeros in C using the minimum number of horizontal and vertical lines;**Step 4: Test for Optimality;****if** the number of covering lines equals n **then** **return** the optimal assignment P determined from the positions of the zeros in C ;**end****else****Step 5: Adjust the Matrix;**Find the smallest uncovered value k in C ;**for** each element $C(i, j)$ that is **not** covered by any line **do** $| C(i, j) \leftarrow C(i, j) - k;$ **end****for** each element $C(i, j)$ that is covered **twice** (i.e., by both a row and a column) **do** $| C(i, j) \leftarrow C(i, j) + k;$ **end****Return to Step 3;****end**

Appendix E. SHAP Results

The following Figure 2 shows the SHAP results for sex classification on tracts.

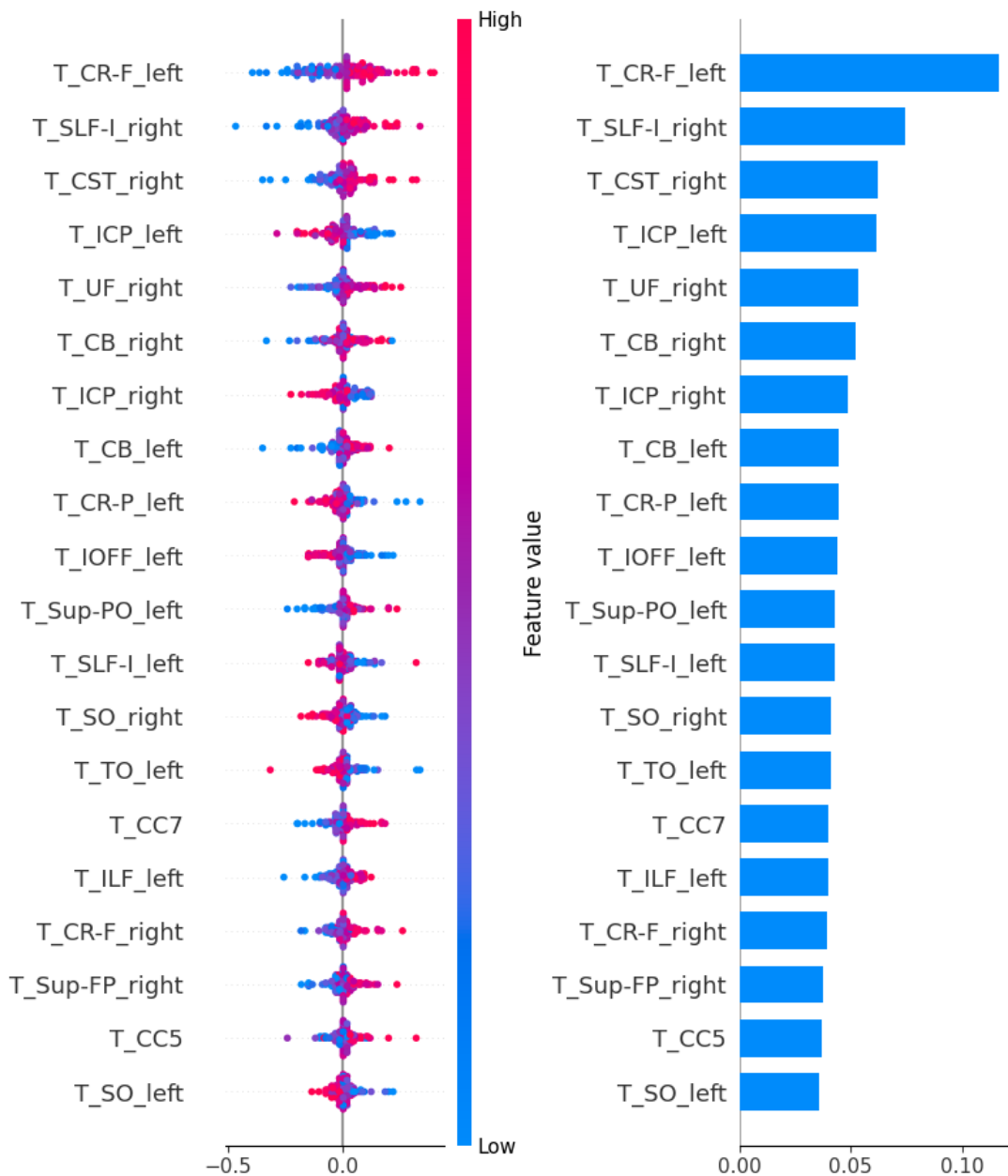


Figure 2: Graph that shows the impact of a tract (right) and the polarity of the interaction with the target i.e. sex classification (left).